British Journal of Cancer www.nature.com/bjc

ARTICLE

Cellular and Molecular Biology

Metabolic stress induces GD2$^+$ cancer stem cell-like phenotype in triple-negative breast cancer

Appalaraju Jaggupilli[1,7], Stanley Ly[1,7], Khoa Nguyen[1], Vivek Anand[1], Bin Yuan[1], Fouad El-Dana[1], Yuanqing Yan[2], Zoe Arvanitis[1], Danthasinghe Waduge Badrajee Piyarathna[3], Nagireddy Putluri[3], Helen Piwnica-Worms[4], Henry Charles Manning[5], Michael Andreeff[1] and V. Lokesh Battula[1,6]✉

BACKGROUND: Metabolic stress resulting from nutrient deficiency is one of the hallmarks of a growing tumour. Here, we tested the hypothesis that metabolic stress induces breast cancer stem-like cell (BCSC) phenotype in triple-negative breast cancer (TNBC).
METHODS: Flow cytometry for GD2 expression, mass spectrometry and Ingenuity Pathway Analysis for metabolomics, bioinformatics, in vitro tumorigenesis and in vivo models were used.
RESULTS: Serum/glucose deprivation not only increased stress markers but also enhanced GD2$^+$ BCSC phenotype and function in TNBC cells. Global metabolomics profiling identified upregulation of glutathione biosynthesis in GD2^{high} cells, suggesting a role of glutamine in the BCSC phenotype. Cueing from the upregulation of the glutamine transporters in primary breast tumours, inhibition of glutamine uptake using small-molecule inhibitor V9302 reduced GD2$^+$ cells by 70–80% and BCSC characteristics in TNBC cells. Mechanistic studies revealed inhibition of the mTOR pathway and induction of ferroptosis by V9302 in TNBC cells. Finally, inhibition of glutamine uptake significantly reduced in vivo tumour growth in a TNBC patient-derived xenograft model using NSG (non-obese diabetic/severe combined immunodeficiency with a complete null allele of the IL-2 receptor common gamma chain) mice.
CONCLUSION: Here, we show metabolic stress results in GD2$^+$ BCSC phenotype in TNBC and glutamine contributes to GD2$^+$ phenotype, and targeting the glutamine transporters could complement conventional chemotherapy in TNBC.

British Journal of Cancer (2022) 126:615–627; https://doi.org/10.1038/s41416-021-01636-y

INTRODUCTION

Triple-negative breast cancer (TNBC) is an aggressive breast cancer subtype with a high risk of recurrence and metastasis. TNBC confers poor outcomes compared with other breast cancer subtypes due to its distinctive clinical and molecular characteristics. The lack of HER2 protein and hormone receptors on the surface of tumour cells limit options for targeted therapy [1, 2].

A rapidly growing tumour needs a constant supply of micronutrients to maintain bioenergetics and biosynthesis of macromolecules [3]. However, this phenomenon confines the supply of nutrients within the tumour microenvironment [3, 4]. Under these nutrient-deprived (ND) conditions, tumour cells tend to undergo metabolic reprogramming and develop alternative approaches to survive [4, 5]. According to the Warburg effect, tumours are highly dependent on glycolysis [6]. However, glucose-deprived conditions limit the entry of glucose-derived metabolites into the tricarboxylic acid (TCA) cycle, resulting in metabolic and oxidative stress [7–9]. Consequently, tumour cells rely on other metabolites such as glutamine as an alternate source [10–12]. Glutamine enters the cell predominantly through glutamine transporters and gets converted to glutamate by the mitochondrial enzyme glutaminase [13–15]. Glutamate contributes to the synthesis of glutathione (GSH) and maintains the homeostasis of reactive oxygen species (ROS) [10, 16, 17]. Given these essential roles of glutamine, inhibition of glutaminolysis has been an effective therapeutic target. A small-molecule inhibitor of glutaminase (CB-839) is being evaluated in clinical studies for cancer patients [12, 13, 17, 18]. However, the role of glutamine on the breast cancer stem-like cell (BCSC) phenotype in TNBC is not known and the inhibition of glutamine transporters in BCSCs is poorly studied [11, 19].

We hypothesise that metabolic stress associated with tumour progression induces a BCSC phenotype in TNBC cells. BCSCs constitute a small fraction of cells in the primary tumour that are relatively quiescent, with stem cell-like properties such as self-renewal capacity exhibiting drug resistance and metastatic potential [20, 21]. We have recently reported ganglioside GD2 as

[1]Section of Molecular Hematology and Therapy, Department of Leukemia, The University of Texas MD Anderson Cancer Center, Houston, TX, USA. [2]Department of Neurosurgery, McGovern Medical School, The University of Texas Health Science Center, Houston, TX, USA. [3]Department of Molecular and Cell Biology, Baylor College of Medicine, Houston, TX, USA. [4]Experimental Radiation Oncology, The University of Texas MD Anderson Cancer Center, Houston, TX, USA. [5]Center for Molecular Probes, Vanderbilt University Institute of Imaging Science, Nashville, TN, USA. [6]Section of Translational Breast Cancer Research, Department of Breast Medical Oncology, The University of Texas MD Anderson Cancer Center, Houston, TX, USA. [7]These authors contributed equally: Appalaraju Jaggupilli, Stanley Ly. ✉email: vbattula@mdanderson.org

Received: 14 April 2021 Revised: 25 October 2021 Accepted: 9 November 2021
Published online: 22 November 2021

a BCSC marker that selectively identifies $CD44^{high}/CD24^{low}$ BCSCs in TNBC and it is upregulated in TNBC patient samples [22–24]. GD3 synthase (gene name *ST8SIA1*), a key player in the biosynthesis of GD2, is highly upregulated in $GD2^+$ BCSCs and knockout of *ST8SIA1* led to complete tumour growth inhibition [24, 25]. Despite these studies, the metabolism of $GD2^+$ BCSCs remains relatively unexplored [26]. In this report, we evaluated the effect of nutrient deprivation on the $GD2^+$ phenotype in TNBC cells and investigated the role of glutamine in BCSC maintenance and function. Moreover, we tested the effects of inhibition of glutamine uptake using a novel inhibitor of neutral amino acid transporters (V9302) on targeting BCSCs in vitro and in vivo.

MATERIALS AND METHODS

Cell culture

Human breast cancer cell lines SUM159 and MDA-MB-231 were cultured in Dulbecco's modified Eagle's medium (DMEM) with 10% foetal bovine serum (FBS) and 1% penicillin/streptomycin. For mimicking nutrient deprivation, cells were cultured with or without medium replacement daily until cells reached >90% confluency. For serum-deprivation experiments, cells were cultured with either 1% or 10% FBS. For glucose-deprivation experiments, DMEM without glucose was used in the presence or absence of glucose (6 g/L), but supplemented with 10% dialysed FBS. For glycolysis inhibition, cells were cultured with or without 2-deoxy-D-glucose (2-DG; 10 mM). Furthermore, to observe the effect of metabolic stress on the induction of BCSC phenotype in non-stem cells, $GD2^-$ cells from SUM159 and MDA-MB-231 cells were flow-sorted and cultured for 5 days with or without 2-DG, as well as in the presence of 1 or 10% FBS. To determine the effect of glutamine on BCSC phenotype and function, cells were cultured with or without L-glutamine at different concentrations. To inhibit glutamine uptake, V9302 (synthesised in Dr. Henry Manning's lab or purchased from Selleck Chemicals) was used at different concentrations. To study the chemotherapeutic effect on the gene expression of glutamine transporter (Solute Carrier Family 1 Member 5, *SLC1A5*), SUM159 and MDA-MB-231 were treated with paclitaxel or doxorubicin at different concentrations for 48 h. The compounds were diluted from 50 mM dimethyl sulfoxide (DMSO) stocks in a complete medium. Cells were routinely checked for the presence of mycoplasma using the Mycoplasma PCR Detection Kit (Applied Biological Materials). To confirm purity, all cell lines are fingerprinted every 6 months at the MD Anderson's Characterized Cell Line Core.

Flow cytometry

After treatment such as serum deprivation, glucose deprivation, 2-DG, glutamine or V9302, SUM159 or MDA-MB-231, cells were trypsinized and collected (at least 0.5×10^6 cells per flow tube). Cells were washed with 1× phosphate-buffered saline (PBS) and incubated with 3 µL of allophycocyanin-conjugated anti-GD2 antibody (Cat# 357306; BioLegend) for 30 min on ice in the dark. After incubation, the cells were washed with fluorescence-activated cell sorting (FACS) buffer containing 1 µg/mL of 4′,6-diamino-2-phenylindole (DAPI; Cat# D1306, Thermo Fisher Scientific) to exclude the dead cells and analysed for GD2 expression using LSR II (BD Biosciences) or Gallios (Beckman Coulter) flow cytometers. Data from 10,000 events were collected and further analysed using the FlowJo 10.7.1 software (FlowJo, LLC).

Metabolomic studies

To identify the metabolic pathways associated with the $GD2^+$ phenotype, five sets of samples were prepared. Each set consisted of a $GD2^{low}$ and a $GD2^{high}$ cell type, as follows: Set 1: *ST8SIA1*-knockout SUM159 cells vs. Cas9 control SUM159 cells [25], Set 2: SUM159 cells cultured with NR vs. ND medium, Set 3 and Set 4: FACS-sorted $GD2^-$ vs. $GD2^+$ SUM159 cells and MDA-MB-231 cells [25] and Set 5: luminal cell-derived (BT-474, MCF-7, MDA-MB-453, SKBR3, T47-D and ZR-75-1) vs. basal cell-derived (SUM159, MDA-MB-231 and MDA-MB-436) breast cancer cell lines. Metabolites were extracted from each set as previously described [27, 28]. The samples were analysed using high-performance liquid chromatography (HPLC) coupled to Agilent 6490 QQQ mass spectrometry using positive and negative electrospray ionisation. The data were processed on MassHunter quantitative analysis software. The identified metabolites were normalised with isotopically labelled internal standard and log 2-transformed on a per-sample, per-method basis. Two-sample *t* tests were performed on every metabolite in the normalised data to compare expression levels between different groups. Differential metabolites were identified by adjusting the *p* values for multiple testing at a false discovery rate threshold of <0.25, and a heat map was generated. A total of 300 metabolites were targeted and differentially regulated in each set were identified and analysed by Ingenuity Pathway Analysis.

Mammosphere and in vitro tumorigenesis assays

A mammosphere assay was performed as previously described [25]. Briefly, MDA-MB-231 and SUM159 cells were treated with V9302 at different concentrations and stained with 1 mg/mL of 3-(4,5-dimethylthiazol-2-yl)-2,5-diphenyltetrazolium bromide (MTT) (Alfa Aesar) after 1 week to count the mammospheres [25]. A soft-agar colony formation assay was performed as TNBC cells were treated with or without V9302, or *SLC1A5*-KD cells (5×0^3 cells per well) and cultured in a complete cell culture medium containing 1 and 0.5% low-melting agarose in a dual-layer setting. The cells were cultured at 37 °C with 5% CO_2 for 3 weeks. The colonies were stained with MTT and imaged [25].

Migration assay

Migration assays were performed using 24-well trans-well chambers, using membrane inserts with 8-µm pores (Corning) as described before [25]. Briefly, SUM159 or MDA-MB-231 cells with or without V9302 at different concentrations were seeded (1×10^4 cells per chamber) into the upper chambers. After 8 h at 37 °C, each membrane was carefully removed from the insert, fixed with 2% formalin and stained with DAPI (1 µg/mL) (Life Technologies). Fluorescent images were captured using the EVOS automated microscope (Thermo Fisher Scientific).

Measurement of total GSH and ROS levels

Total GSH was measured using a Glutathione Assay Kit (Cayman Chemicals) according to the manufacturer's instructions. SUM159 or MDA-MB-231 cells were treated with or without V9302 for 72 h following the procedure for adherent cells as per the manufacturer's instructions. The total GSH concentration of the samples was measured by the end-point method at 405–414 nm using a VICTOR X3 automated plate reader (Perkin-Elmer). To measure total ROS levels, the cells were incubated with a ROS detection reagent available in the ROS-ID Total ROS Detection Kit (Enzo Life Sciences). ROS levels were determined by LSR II flow cytometry as per the manufacturer's instructions.

Detection of lipid peroxidation-induced ferroptosis

Ferroptosis was detected as previously described [29]. Briefly, TNBC cells (1×10^6 cells/well in 6-well plates) were treated with either V9302 (5, 10 or 20 µM) or *tert*-butyl hydroperoxide (100 µM) (Sigma) with or without ferroptosis inhibitor ferrostatin-1 (Ferr-1, 0.5 µM) (Sigma) for 48 h at 37°C with 5% CO_2. C11-BODIPY (10 µM, Thermo Fisher Scientific) was then added and incubated for 20 min at 37 °C. All the cells were collected and analysed by flow cytometry using the fluorescein isothiocyanate channel. For the measurement of in vivo lipid peroxidation, patient-derived xenograft (PDX) tumours were disaggregated into a single-cell suspension, immediately incubated with C11-BODIPY and prepared for flow cytometry. Ten thousand events were collected and analysed by the FlowJo software.

Generation of *SLC1A5*-knockdown cells

Lentiviral-mediated short hairpin RNA (shRNA) was used to stably knock down *SLC1A5* in SUM159 cells as described before [30]. The shRNA constructs were purchased from Horizon Discovery (sequencing primer: 5′-AAACCCAGGGCTGCCTTGGAAAAG-3′, vector map: pLKO.1, NM_001145144.2; NM_001145145.2; NM_005628.3; clone ID: TRCN0000043121). Lentiviral pLKO.1 vector (GE-Dharmacon) was used as a scramble control. To select the transduced cells, the medium was replaced with DMEM containing puromycin (1 µg/mL) (InvivoGen). Knockdown efficiency was quantified by quantitative PCR (qPCR) and Western blotting (ASCT2 antibody; Cat# PA5-83265; Thermo Fisher), respectively.

Western blotting

For western blotting, the cells were lysed and proteins were extracted as described previously [25]. The membranes were incubated with the primary antibodies overnight at 4 °C (Supplementary Table 1). The membranes were then washed and incubated with donkey anti-mouse immunoglobulin G antibody conjugated with Alexa Fluor 680 or donkey anti-rabbit antibody

conjugated with Alexa Fluor 800 (Cat# A10038 and A32808; Thermo Fisher Scientific). The membranes were washed again and scanned using the ChemiDoc Imaging System (Bio-Rad) or Odyssey Fluorescence Imaging System (LI-COR Biosciences).

Real-time qPCR

RNA extraction was performed using RNeasy Mini Kit (Qiagen) following the manufacturer's instructions. The complementary DNA for each sample was synthesised using 1 µg of RNA and SuperScript IV VILO Master Mix (Invitrogen). Real-time qPCR was performed using the TaqMan gene expression assay (Applied Biosystems). The primers used were provided in Supplementary Table 2. Relative messenger RNA expression was normalised to glyceraldehyde 3-phosphate dehydrogenase expression.

Animals

All experiments involving animals were approved by and conducted in accordance with the policies of the Institutional Animal Care and Use Committee (IACUC) of The University of Texas MD Anderson Cancer Center. Female NSG mice (non-obese diabetic/severe combined immunodeficiency with a complete null allele of the IL-2 receptor common gamma chain [*IL2rg*^{null}]; 8 weeks old) were housed in the plastic cages in groups of five and allowed a week to adapt to the housing facility. Animals were supplied with rodent maintenance food, water and inspected twice daily. At the end of the experiment, the animals were humanely euthanized per IACUC guidelines by placing them in a euthanasia chamber and providing CO_2 using a gauge and pressure regulator. As a secondary physical method, cervical dislocation was performed after euthanasia. No anaesthesia was given during this procedure.

In vivo tumour growth

shRNA control or *SLC1A5*-KD SUM159 cells (1×10^6) were resuspended in ECMatrix solution (EMD Millipore) and implanted into the mammary fat pads of NSG mice ($n = 10$; 5 mice per group). Once the tumours were palpable at week 3, tumour volumes were measured using callipers every week until the tumours reached 2 cm in diameter. To study the effect of V9302 on tumour growth, TNBC PDX cells (PIM 005, 3×10^6) were implanted into the mammary fat pads of NSG mice ($n = 20$; 5 mice per group) [31]. Once the tumours were palpable after week 4, the mice were randomly divided into four groups. Treatments and measurements were performed serially based on cage number and this order was maintained throughout the study. However, any other potential confounders were not controlled for. From week 5, each group of mice were treated with V9302 (15 mg/kg/day) or vehicle control (2% DMSO in PBS) three times a week (Monday, Wednesday and Friday). Each week, tumour volumes were measured using callipers and mouse body weights were measured using a simple balance. When the tumour reached 2 cm in diameter, the mice were sacrificed. The tumours were harvested from both groups, minced and digested using collagenase III (Sigma) and dispase (Stemcell Technologies) to obtain single-cell suspensions.

Statistics

METABRIC dataset (cBioPortal database), comprising 2509 breast cancer samples (including 199 basal, 199 claudin-low, 220 HER2, 679 luminal A and 461 luminal B) and 140 normal-like adjacent breast tissues was used to analyse different glutamine transporters genes. Differential expression between the subgroups was tested by using one-way analysis of variance (ANOVA) with Tukey's honestly significant difference post hoc test. The Kaplan–Meier method was used to plot survival curves and was evaluated by the log-rank test. All the statistical analysis was conducted in R software (version 3.5.3), and p values <0.05 were considered statistically significant. For synergism analysis, the cells were treated with V9302 or paclitaxel or both for 72 h. The combination index (CI) was evaluated by the CompuSyn software. Dose–response curves from combined treatment were fitted to Chou–Talalay lines, which were derived from the law of mass action. CI < 1 indicates synergistic interaction; CI = 1, additive interaction; and CI > 1, antagonistic interaction. All other statistical analyses were performed using GraphPad Prism software (version 8.2.1). Unless otherwise indicated, the data shown represent the mean ± standard deviation. The statistical significance between two-sample groups was analysed by unpaired t test; for three or more groups, one-way ANOVA was used. Differences within the treatment groups were analysed with two-way ANOVA. For in vivo experiments, one-way ANOVA followed by Bonferroni's multiple comparison test was performed for tumour volumes, and an unpaired t test was performed for the tumour weights.

RESULTS

Nutrient/glucose deprivation induces a GD2$^+$ BCSC phenotype in TNBC cells

To study the effect of nutrient deprivation on the CSC phenotype, SUM159 and MDA-MB-231 cells were cultured with or without fresh media replacement on daily basis to mimic gradual nutrient deprivation in the tumour microenvironment. GD2 expression was analysed prior to seeding and at 24-h intervals after seeding. Interestingly, on day 5, SUM159 cells with fresh media had a lower number of GD2$^+$ cells (15 ± 1.5%) compared with cells without media replacement (33 ± 2.5%), and the same was found for MDA-MB-231 cells (4 ± 0.5% compared with 15 ± 0.5%) (Fig. 1a, b). These data suggest that nutrient deprivation could induce a GD2$^+$ stem cell phenotype. In further validations with nutrient-rich (NR, 10% serum) or ND (1% serum) medium, both cell lines showed a percentage of ~20% GD2$^+$ cells at the end of 4 days in NR, compared with ~50% in ND medium (Fig. 1c). To determine whether the increase in GD2$^+$ cells under metabolic stress is a true induction of stem cell-like phenotype, but not the expansion of the residual GD2$^+$ cells, we sorted GD2$^-$ cells from SUM159 and MDA-MB-231 cells and cultured them with or without glycolysis inhibitor 2-DG or medium with 1 or 10% FBS for 5 days. Both SUM159 and MDA-MB-231 cells showed a significant increase ($p < 0.05$) in their percentage of GD2$^+$ cells when cultured in the presence of 2-DG (from 1.64 to 5.63% in SUM159 cells and from 0.84 to 4.68% in MDA-MB-231 cells) or in the media supplemented with 1% serum (from 1.9 to 11.8% in SUM159 cells and 0.83 to 2% in MDA-MB-231 cells) compared to the cultures in the absence of 2-DG and media supplemented with 10% serum, respectively (Supplementary Fig. 1). Next, to investigate whether nutrient stress induced a GD2$^+$ stem cell in vivo, NSG mice xenograft model with MDA-MB-231 cells was examined for GD2 expression in the implanted tumours once a week (Supplementary Fig. 1a–c). Interestingly, the percentage of GD2$^+$ cells increased from 18 ± 1.5 to 45 ± 2.5% with the tumour growth over a 6-week period (Supplementary Fig. 2b, c), suggesting that the metabolic stress within the tumour induced a GD2$^+$ BCSC phenotype.

Since glucose is an essential source of energy, we tested the effects of glucose deprivation. Interestingly, we observed a 2–3-fold increase in GD2$^+$ cells in a time-dependent manner from 28.77 ±4.87% at 48 h to 33.63 ±4.5% at 96 h in SUM159 and 15.9 ± 1.2% at 48 h to 20.5 ± 1.2% at 72 h in MDA-MB-231 cells in glucose-deprived conditions compared with control conditions (Fig. 1d). Although it was not significant at the 96 h time point for MDA-MB-231 cells; GD2 expression was higher when glucose was deprived. Further validations using 2-DG, which inhibits glycolysis showed a 2–3-fold increase of GD2$^+$ cells (17.7 ± 1.45% at 48 h, 27.2 ± 1.5% at 72 h and 16.05 ± 1.4 at 96 h in SUM159 and 11.9 ± 0.6% at 48 h, 11.65 ± 0.57 at 72 h and 13.5 ± 0.58% at 96 h in MDA-MB-231 cells) compared to control cells (~10% in SUM159 or ranging from 5.4% at 48 h to 10.7% at 96 h in MDA-MB-231 cells) (Fig. 1e). The lower number of GD2$^+$ SUM159 cells at 96 h might be due to saturation of cell growth influencing the phenotype transition. However, there is a significant difference (2-fold) between 2-DG-treated and -untreated cells. Unlike glucose deprivation, 2-DG treatment did not reduce cell viability, which could be due to alternative metabolites present in the FBS (Supplementary Fig. 2d). Taken together, these results suggest that glucose deficiency aids in the conversion/dedifferentiation of GD2$^-$ into GD2$^+$ BCSCs.

Nutrient deprivation induces metabolic stress and enhances BCSC functions in TNBC cells

To validate the effects of nutrient deprivation on metabolic stress in cancer cells, we first examined the expression of metabolic stress markers such as ATF4 and SESN2 in cells cultured in serum/glucose-deprived medium. As expected, expression of ATF4 and

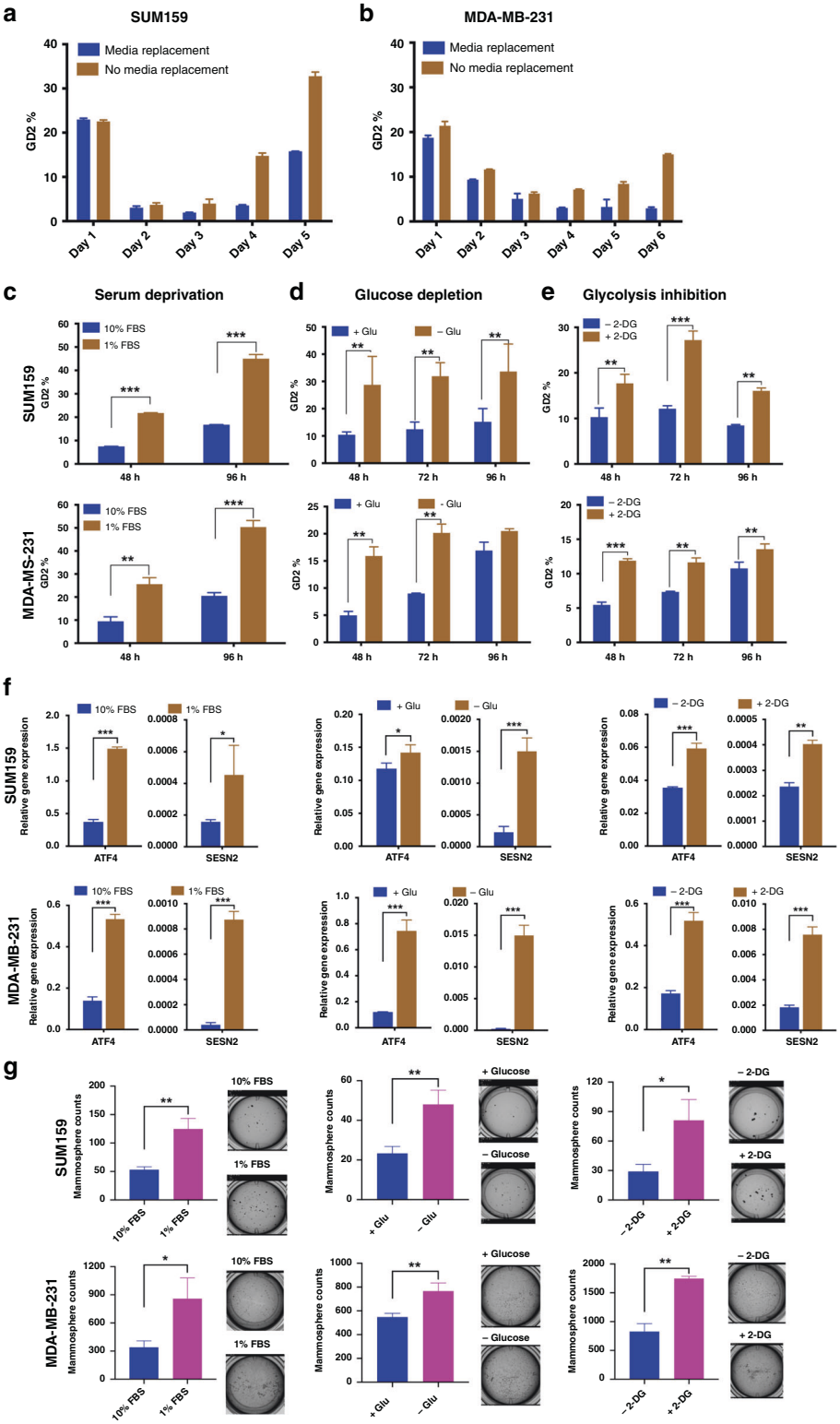

Fig. 1 Serum and glucose deprivation induces GD2 expression in TNBC. a, **b** SUM159 (50,000 cells/well) or MDA-MB-231 (75,000 cells/well) cells were plated in 24-well plates and maintained with or without replacing the cell culture media after initial seeding. GD2 expression was analysed using flow cytometry with APC-conjugated anti-GD2 antibody at 24-h intervals. **c** SUM159 and MDA-MB-231 cells were grown in cell culture media supplemented with either 1 or 10% FBS for 24 and 48 h. **d** For glucose deprivation, SUM159 and MDA-MB-231 cells were grown in dialysed FBS supplemented with or without glucose for 48, 72 and 96 h. **e** For glycolysis inhibition, SUM159 and MDA-MB-231 cells were grown in 10% FBS with or without 2-DG (10 mM) for 48, 72 and 96 h. GD2 expression was analysed using flow cytometry after every time point as indicated. **f** Gene expression of stress markers (ATF4 and SESN2) in SUM159 and MDA-MB-231 cells cultured under serum deprivation, glucose depletion and glycolysis inhibition for 48 h. **g** Mammosphere formation from the cells cultured under serum deprivation, glucose depletion and glycolysis inhibition. Two-way ANOVA followed by Sidak's post hoc multiple comparison test was performed for GD2 expression between the treatment groups. ***$p = 0.001$, **$p = 0.002$ and *$p = 0.033$. An unpaired t test was performed to calculate the significance for gene expression of stress markers and mammosphere counts; ***$p = 0.001$, **$p = 0.002$ and *$p = 0.033$.

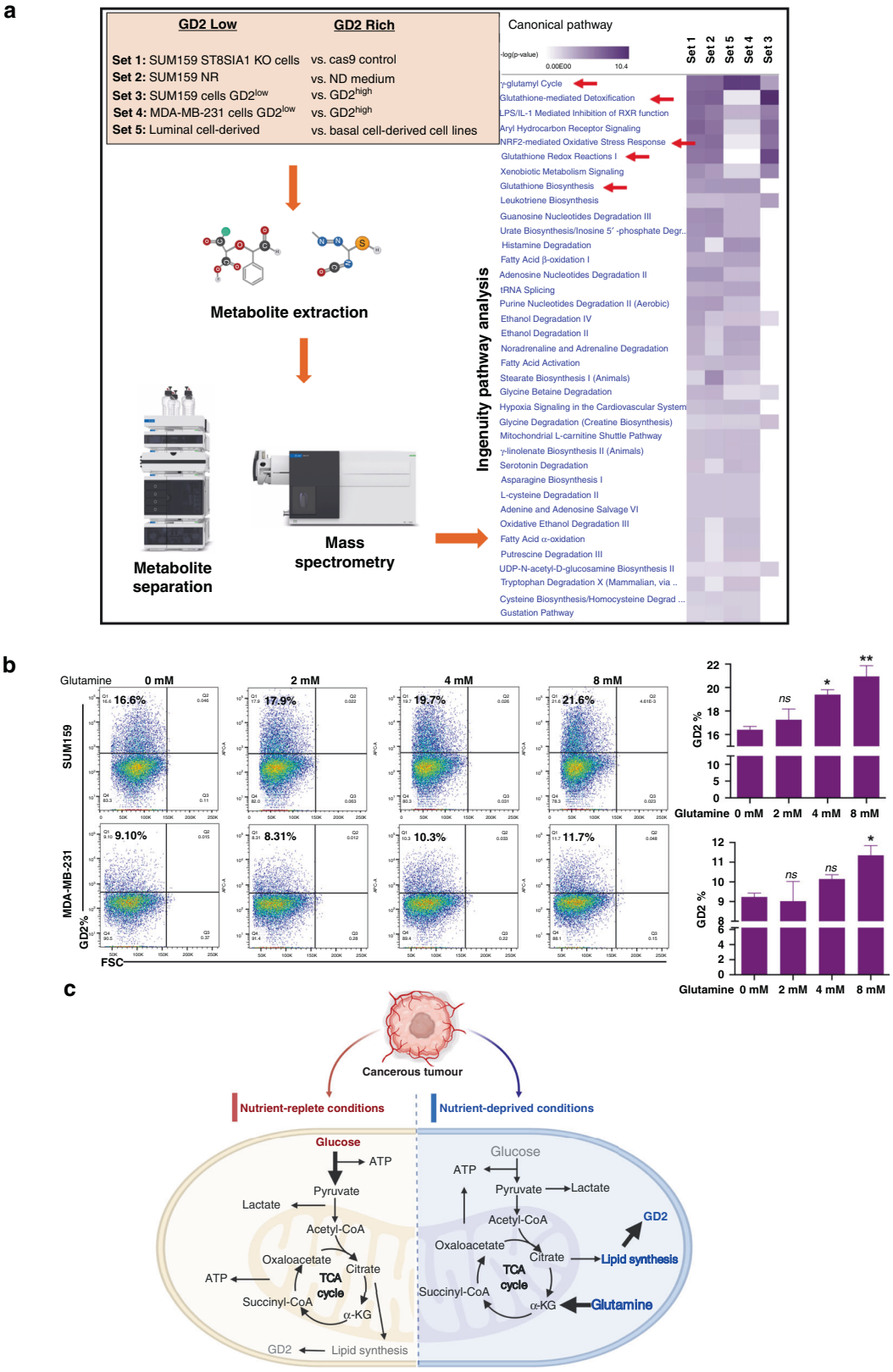

SESN2 was induced under metabolic stress in both SUM159 (2–3-fold) and MDA-MB-231 (2–4-fold) cells (Fig. 1f). In addition, we also observed that the mammosphere-forming capabilities were significantly enhanced when cells were grown under serum- or glucose-deprived conditions (2.5-fold in SUM159 and 1.5–3-fold in MDA-MB-231; Fig. 1g). In corroboration to the in vitro (Supplementary Fig. 1) and in vivo results (Supplementary Fig. 2b, c), these data suggest that TNBC cells can adapt to nutrient deprivation-mediated metabolic stress by inducing a $GD2^{+}$ BCSC phenotype.

Fig. 2 Metabolomic profiling of breast cancer stem cells. a TNBC cell lines MDA-MB-231 and SUM159 were subjected to different conditions, and metabolomics profiling of >300 metabolites was performed using a mass spectrometry-based assay. The resulting data were analysed in five different sets as shown and described in 'Materials and methods'. Samples were subjected to metabolite extraction followed by purification and mass spectrometry analysis. The elevated pathways were identified using Ingenuity Pathway Analysis. **b** Glutamine regulates GD2 expression in TNBC cells. TNBC cell lines SUM159 (3×10^5/well) and MDA-MB-231 (4.5×10^5/well) in 12-well plates were cultured with increasing concentrations of L-glutamine (0, 2, 4 and 8 mM) for 72 h and GD2 expression was measured by flow cytometry. One-way ANOVA followed by Dunnett's post hoc multiple comparison test was performed for GD2 expression, taking untreated cells as the control. $^{**}p = 0.006$, $^{*}p < 0.05$ and n.s. not significant. **c** Illustration of nutrient-replete and nutrient-deprived conditions regulating GD2 expression. The left-side panel represents glucose-rich conditions (bold arrow) to maintain an optimal level of GD2 in a stress-free environment. The right-side panel depicts glucose depletion in metabolic stress conditions leading to an upregulation of GD2 expression by utilising the glutamine-mediated pathways (bold arrow). Grey colour represents low levels and blue represents higher levels of metabolites.

Glutamine upregulates GD2 expression in TNBC cells

Since serum or glucose deprivation induced the $GD2^+$ phenotype in TNBC cells, we conducted global metabolic profiling of TNBC cells to understand the alternate metabolic processes in $GD2^+$ cells. TNBC and non-TNBC cells were grouped into five different sets based on the levels of GD2 expression (Fig. 2a). The targeted mass spectrometry detected metabolites associated with GSH metabolism, including glutamyl-alanine, 5-oxy-proline, proline, glutamine and GSH itself, were highly upregulated in $GD2^{high}$ cell types (Supplementary Data Set 1). Ingenuity Pathway Analysis of differentially expressed metabolites revealed that GSH-mediated detoxification, GSH redox reactions and GSH biosynthesis are the top canonical pathways highly associated with $GD2^+$ cells (Fig. 2a). These data suggest that GSH-mediated pathways play a key role in the $GD2^+$ BCSC phenotype. Since glutamine is a major precursor for GSH biosynthesis, we speculated that glutamine contributes to GD2 biosynthesis and tested the involvement of glutamine. The percentage of $GD2^+$ cells significantly increased from 16.4 ± 0.28 to $21 \pm 0.91\%$ in SUM159 cells and from 9.25 ± 0.2 to $11.35 \pm 0.49\%$ in MDA-MB-231 cells with increasing concentration of glutamine (Fig. 2b). These results indicate that glutamine may directly contribute to GD2 biosynthesis through the TCA cycle and lipid synthesis (Fig. 2c).

Upregulation of glutamine transporters is associated with poor overall survivability in breast cancer patients

Based on the above results, we focused on the expression of glutamine transporters in breast cancer patients. METABRIC breast cancer patient data analysis showed a significant upregulation of *SLC1A5* in basal, HER2 and luminal A breast cancer subtypes ($p < 0.05$) compared to normal-like adjacent breast tissue (Fig. 3a). Also, significant upregulation of *SLC1A5* in stage 2 and 3 tumours compared to stage 1 suggests an association of *SLC1A5* expression with disease progression ($p < 0.05$) and ($p < 0.001$), respectively (Fig. 3b). In addition, *SLC1A5* is upregulated in the TNBC subtype ($p = 0.015$; Fig. 3c), which was also supported by our in vitro analysis of *SLC1A5* expression in different breast cancer cells ($p < 0.05$) (Supplementary Fig. 2a). However, *SLC1A5* expression showed no difference among the subtypes of TNBC (Supplementary Fig. 3a). Moreover, metastatic tumours ($p = 0.0003$; Fig. 3d) and patients treated with chemotherapy ($p = 0.003$; Fig. 3e) showed higher *SLC1A5* expression compared to their respective controls. Our in vitro validation with paclitaxel and doxorubicin has significantly increased *SLC1A5* in SUM159 and MDA-MB-231 cells (Supplementary Fig. 3c–f). Furthermore, high *SLC1A5* expression is associated with poor overall survival in breast cancer patients ($p < 0.00001$; Fig. 3f). Collectively, the expression analysis emphasises the role of the predominant glutamine transporter (ASCT2) in the progression of breast cancer and chemotherapy resistance. Our further analysis on the other glutamine transporters showed that 50% of the SLC38A (SNAT) family (SLC38A3, 5, 7, 8 and 10) and SLC7A5 (LAT1) are upregulated in TNBC patients suggesting their significance in TNBC progression (Supplementary Fig. 3g, h).

Next, to examine the effects of inhibition of glutamine uptake on in vivo tumour growth, we knocked down *SLC1A5* in SUM159 cells (Supplementary Fig. 3i, j). Knockdown of *SLC1A5* in SUM159 cells decreased GD2 expression by 45% and soft-agar colony formation by 2-fold compared to the scramble control (Fig. 3g, h), suggesting the importance of glutamine uptake in the maintenance of $GD2^+$ BCSC phenotype. In vivo studies using *SLC1A5*-KD SUM159 showed a significant reduction of tumour volume ($p < 0.001$) in the xenograft mice model compared to mice injected with scramble control cells (Fig. 3i). This support our in vitro data emphasising the significance of glutamine transport for BCSC phenotype and tumour growth.

Inhibition of glutamine uptake regulates GD2 expression and BCSC functions

As glutamine transporters facilitate glutamine uptake for BCSC function, we, therefore, used V9302, a small-molecule inhibitor of glutamine transporters [32–34]. Although its specificity remains debatable, here our objective is to understand the effects of inhibition of glutamine uptake on $GD2^+$ BCSC phenotype. Interestingly, V9302 treatment on SUM159 and MDA-MB-231 cells resulted in ~70–80% reduction of GD2 expression in a dose-dependent manner (Fig. 4a, h and Supplementary Fig. 4a). This strengthens our case that glutamine is an essential metabolite for GD2 biosynthesis.

Next, to determine the effect of V9302 on BCSC function, we tested the ability of TNBC cells to form soft-agar colonies and mammospheres and to undergo migration in vitro. Interestingly, V9302 reduced soft-agar colonies (Fig. 4b, i and Supplementary Fig. 4b) and mammosphere formation (Fig. 4c, j and Supplementary Fig. 4c) by 70–90% in both SUM159 and MDA-MB-231 cells. We also assessed the readout of stem cell counts post V9302 treatment. Prior treatment of SUM159 and MDA-MB-231 cells with V9302 for 72 h before seeding cells for mammosphere assay also inhibited mammosphere development in a dose-dependent manner, with the greatest effect at 20 μM concentration (Supplementary Fig. 4d). In addition, V9302 also inhibited the migration of TNBC cells (Fig. 4d, k). Together, these data indicate that inhibition of glutamine uptake greatly reduces BCSC functionality. Our further assessment of inhibition of glutamine uptake under glucose-deprived conditions V9302 reduced the GD2 expression in cells treated with 2-DG (Fig. 4e, l and Supplementary Fig. 4e), suggesting that TNBC cells acquire $GD2^+$ BCSC phenotype by consuming more glutamine under glucose-deprived conditions.

V9302 disrupts redox homeostasis in TNBC cells

Since glutamine is the main precursor for glutamate and GSH synthesis, we investigated the downstream mechanistic effects of V9302 on the regulation of GSH and ROS levels in TNBC cells. V9302 treatment reduced total GSH in a concentration-dependent manner in both SUM159 and MDA-MB-231 cells (Fig. 4f, m). In addition, the V9302 treatment increased ROS levels in both cell lines (Fig. 4g, n). These data indicate that V9302 targeting glutamine transporters reduce GSH synthesis and downregulates GSH-mediated redox homeostasis, strengthening their potential as therapeutic targets in TNBC treatment.

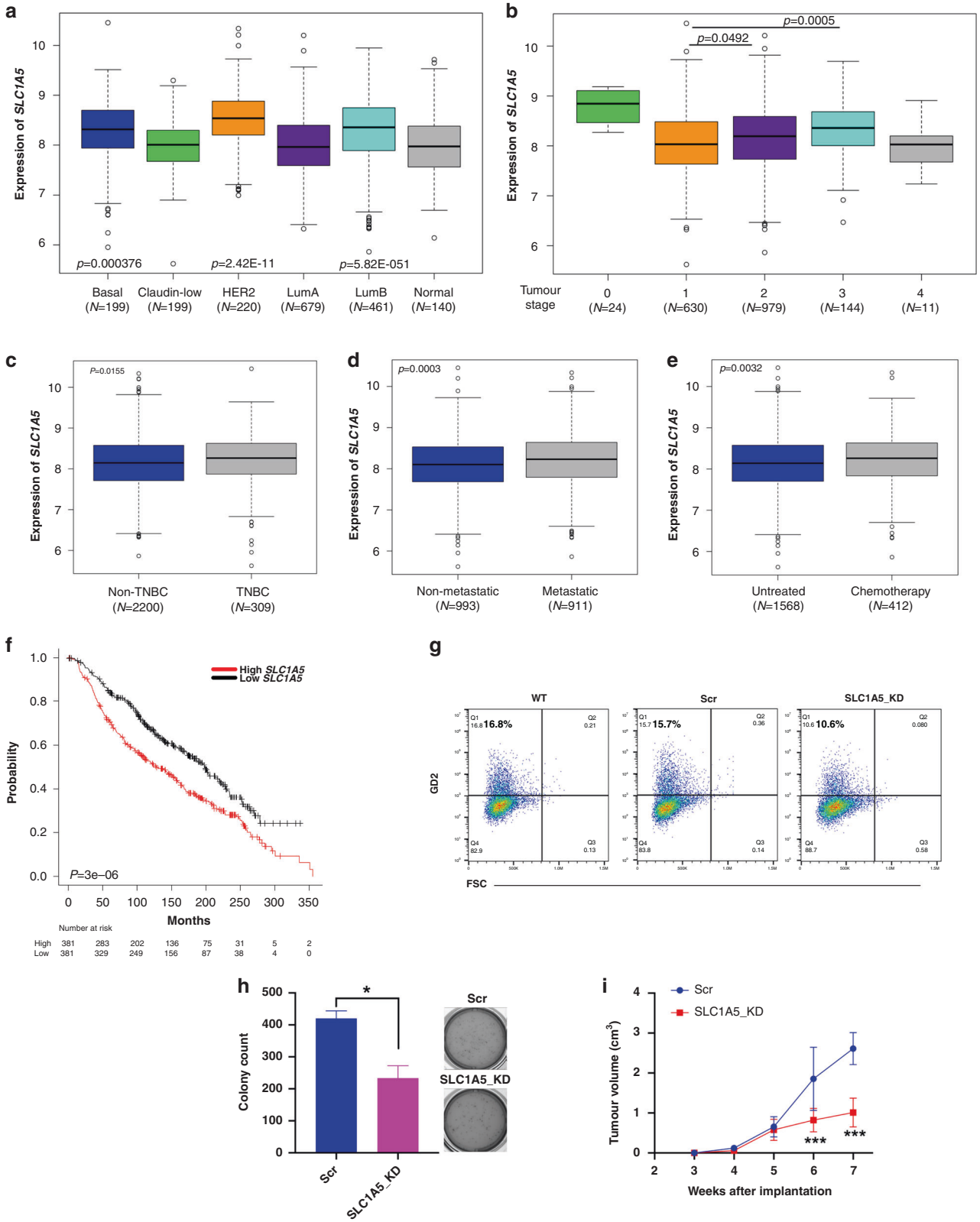

V9302 synergises with paclitaxel in inducing cell death in TNBC

Since inhibition of glutamine uptake reduces GSH levels, we hypothesised that V9302 induces synergistic killing of TNBC cells when combined with chemotherapeutic agents. We tested the combination of V9302 with paclitaxel. At a high concentration (20 μM), V9302 induced 30% cell death, while paclitaxel induced 20–90% cell death in a dose-dependent manner in both SUM159 and MDA-MB-231 cells (Fig. 5a, b). The combination of both compounds induced 80–90% cell death at higher concentrations.

Fig. 3 METABRIC dataset show higher expression of *SLC1A5* in breast cancer patients and is associated with poor survivability. METABRIC dataset was retrieved from the cBioPortal database and grouped into different clinical attributes for the comparative analysis. **a** Expression of *SLC1A5* in different subtypes of breast cancer. With $p < 0.05$, higher expression was observed in basal, HER2 and luminal B in comparison with normal-like adjacent breast tissues. **b** Comparison of *SLC1A5* expression at different stages of breast cancer. With a very low sample number, stages 0 and 4 were excluded from the statistical analysis. One-way ANOVA followed by Tukey's HSD post hoc test was performed. **c** Comparison of expression of SLC1A5 between non-TNBC and TNBC patient samples, **d** non-metastatic and metastatic patient samples, **e** untreated and chemotherapy. Unpaired Student's *t* test was performed with $p < 0.05$ statistically significant. The data represent mean ± standard deviation. **f** The Kaplan–Meier survival curves compare the outcomes of patients with high (red) and low (black) expression of *SLC1A5*, divided by the median value, among the 762 breast cancer patients. **g** Flow cytometry analysis of GD2 expression in *SLC1A5*-KD and shRNA control cells. **h** Soft-agar colony formation of *SLC1A5*-KD and shRNA control cells. An unpaired *t* test was performed between untreated and V9302-treated tumour cells. *$p = 0.033$. **i** *SLC1A5*-KD and shRNA control SUM159 cells were implanted (1×10^6 per mouse) into the mammary fat pads of NSG mice ($n = 10$, 5 mice per group). Tumour volume was measured every week; shown are tumours at the end of the experiment 7 weeks after implantation. ***$p < 0.001$.

V9302 exhibited synergism at 5–20 μM with paclitaxel at 0.625–10 nM, with CIs <1 (Fig. 5c, d). Collectively, a significant increase in cell death suggests the potential of V9302 in combination with chemotherapeutic agents in TNBC treatment.

Reduced levels of the antioxidant GSH may induce ROS-mediated cancer cell death. Therefore, to investigate the mechanism of V9302-mediated cell death, TNBC cells were treated with various concentrations of V9302, and activation of caspase-9 was measured. Although V9302 treatment induced partial activation of caspase-9 (Supplementary Fig. 5a), there were no significant changes in annexin V binding (Supplementary Fig. 5b), indicating that V9302 may not mediate apoptosis. As GSH is the precursor for GSH peroxidase 4 (GPX4), a regulator of lipid peroxides, we then analysed lipid peroxidation-induced ferroptosis, an iron-dependent means of cell death. Interestingly, V9302 treatment significantly induced C11-BODIPY binding, which detects lipid peroxides, in a concentration-dependent manner from the mean fluorescence intensity of 1661–2350 in SUM159 cells ($p < 0.01$) and 986–1342 in MDA-MB-231 cells ($p < 0.001$). The control treatment with Ferr-1-reduced V9302-induced ferroptosis in both cell lines (Fig. 5e, f and Supplementary Fig. 5c). These results suggest that V9302 induces ferroptosis in TNBC cells.

V9302 inhibits signalling pathways downstream of GD2

Considering GD2-mediated activation of FAK-AKT-mTOR pathway and significance of glutamine metabolism in mTOR-mediated cancer cell growth, we investigated the effects of inhibition of glutamine uptake on mTOR signalling [19, 25, 35]. Western blot analysis showed that 24 h treatment with V9302 significantly reduced phospho-AKT (S473), phospho-ERK (T202/Y204), phospho-mTOR (S2448) and phospho-4E-BP1 (S65) in SUM159 and MDA-MB-231 cells in a dose-dependent manner (Fig. 5g). Consistent with the previous studies, these data demonstrate that inhibition of glutamine uptake negatively regulates signalling downstream of GD2.

In vivo inhibition of glutamine uptake reduces tumour growth

Finally, we tested the effect of V9302 on TNBC tumours in vivo using PDX cells (3×10^6 per mouse) implanted into the mammary fat pads of NSG mice. After palpable tumours were observed after week 5, randomly grouped mice (5 per group) were injected with either V9302 (20 mg/kg) or vehicle (2% DMSO) (Fig. 6a). V9302 showed a significant reduction in the PDX tumour growth from week 6 onwards without affecting the weight of the mice (Fig. 6b–e). In addition, we tested the ability of V9302 to generate in vivo lipid peroxides as a measure of ferroptosis and found significant induction of the C11-BODIPY signal in V9302-treated tumours compared to controls (Fig. 6f). Together, the data suggest that regulation or pharmacological inhibition of glutamine uptake by targeting glutamine transporters decrease in vivo tumour growth while inducing ferroptosis of the tumour cells (Fig. 6g).

DISCUSSION

Building on our prior identification of GD2 as a BCSC marker, here we show that metabolic stress caused by nutrient deprivation induces a $GD2^+$ BCSC phenotype in TNBC. We found that GSH-mediated metabolic pathways are highly upregulated in $GD2^+$ cells and that glutamine acts as a metabolic source for GD2 biosynthesis. Finally, inhibiting glutamine uptake reduced GD2 expression, BCSC function, mTOR pathway signalling and in vivo tumour growth by inducing ferroptosis.

Nutrient deprivation induces metabolic stress and modulates the BCSC phenotype and metastatic potential in breast cancer [4, 36]. Under these conditions, cells tend to adapt and contribute to tumour progression by utilising alternative metabolites [37–39]. Our study suggests the spontaneous adaptation and modulation of the $GD2^+$ BCSC phenotype in response to metabolic stress. Glucose is a major precursor for *N*-acetylneuraminic acid (sialic acid) biosynthesis, contributing its carbons through the hexosamine pathway [40, 41]. Interestingly, sialic acid is the most common glycoside moiety in gangliosides such as GD2 [40, 42]. Targeting the enzymes involved reduced sialic acid levels and impaired lung metastasis [43]. We have previously reported a similar strategy by downregulating *ST8SIA1*, the gene encoding for GD3 synthase and a crucial enzyme in GD2 biosynthesis, to impair tumour growth and metastasis in TNBC [22, 24, 25]. However, GD2 expression was enhanced by glucose depletion and little is known about other factors contributing to the $GD2^+$ BCSC phenotype. A link between glycosphingolipids and glutamine metabolism was recently proposed [44]. Therefore, it is possible that cells depend on both glucose and glutamine metabolism to synthesise gangliosides under normal conditions. Our metabolomics analysis followed by glutamine supplementation revealed the underlining role of glutamine metabolism in GD2 biosynthesis (Fig. 2b). Interestingly, the blockade of glutamine transporters has been gaining traction as druggable targets to control TNBC growth [11, 19]. Recent studies reported that V9302, targeting glutamine uptake reduced tumour volume [32, 34, 45]. Interestingly, an association of ASCT2 with GD2 in glycolipid-enriched microdomain/rafts was studied in small cell lung cancer [46]. However, their study was focused on elucidating that glutamine uptake was elevated in $GD2^+$ compared to $GD2^-$ cells. Here, we show that V9302 inhibited GD2 expression in TNBC cells, in vitro tumorigenesis and in vivo tumour growth, supporting our hypothesis that glutamine metabolism regulates GD2-mediated BCSC functions in TNBC.

Disruption of redox homeostasis through nutrient deprivation-induced ROS levels has been considered for redox-based cancer therapies [47, 48]. In this study, inhibition of glutamine transport disrupted redox homeostasis in TNBC cells. However, the V9302 treatment did not induce apoptosis as expected. TNBC is known to be enriched for a ferroptosis gene signature and is susceptible to ferroptosis [49]. GPX4 is known to be the key regulator of ferroptosis [50]. Thus, we tested V9302 effects and interestingly it induced lipid peroxides suggesting that targeting glutamine

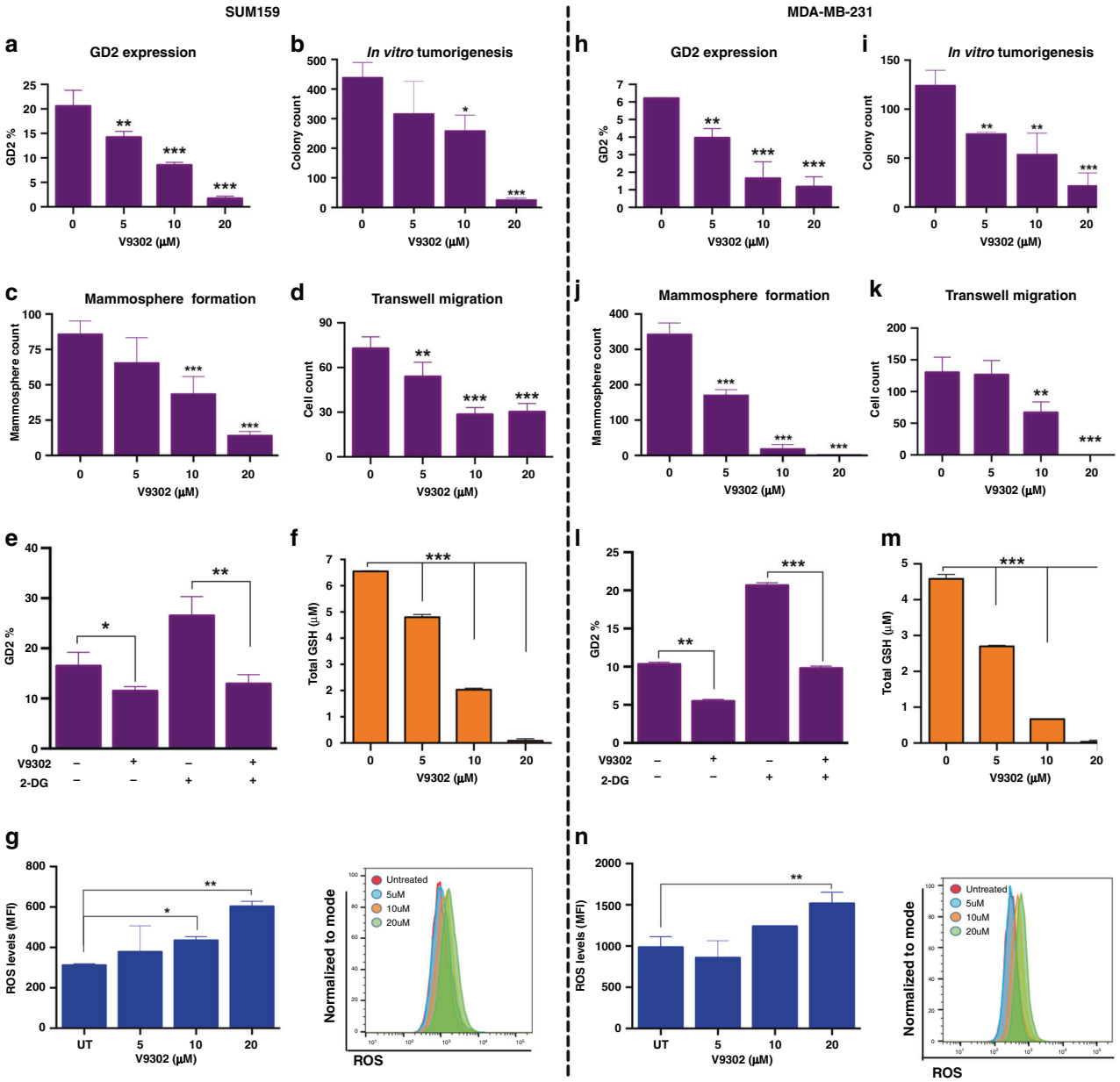

Fig. 4 V9302 inhibits GD2 expression, BCSC function and the glutathione (GSH) pathway in TNBC cells. a, **h** SUM159 (50,000 cells/well) or MDA-MB-231 (75,000 cells/well) were plated in 24-well plate treated with or without V9302 (small-molecule inhibitor of ASCT2) in a dose-dependent manner (0, 5, 10, and 20 μM) for 72 h, and GD2 expression was measured by flow cytometry. **b**, **i** SUM159 or MDA-MB-231 cells (5×10^3 cells/well) were seeded into soft-agar medium containing different concentrations of V9302 (0, 5, 10 and 20 μM). After 3 weeks, the colonies were fixed and stained by the MTT method. Tumorigenesis was assessed by counting the resulting colonies by an automated colony counter. **c**, **j** SUM159 or MDA-MB-231 cells were seeded (5×10^3 per well) into low-adherent dishes containing MammoCult medium with different concentrations (0, 5, 10 and 20 μM) of V9302. After 3 weeks, the mammospheres were stained with MTT reagent and counted by an automated colony counter. **d**, **k** SUM159 or MDA-MB-231 cells were cultured in 24-well trans-well chambers, using membrane inserts with 8-μm pores in DMEM containing 1% FBS. The cells (1×10^4 per chamber) were seeded into the upper chambers for 8 h. Membranes were fixed with 2% formalin and stained with DAPI. Fluorescent images were captured using the EVOS automated microscope. One-way ANOVA followed by Dunnett's post hoc test was performed for GD2 expression, taking untreated cells as the control. ***$p = 0.001$, **$p = 0.002$ and *$p = 0.033$. **e**, **l** Combinatorial effect of V9302 and 2-DG on TNBC cells. SUM159 and MDA-MB-231 cells were treated with either V9302 (10 μM) or 2-DG (10 mM) alone or in combination for 72 h. GD2 expression was analysed using flow cytometry analysis. Unpaired *t* test was performed between untreated and V9302-treated cells in the presence or absence of 2-DG. ***$p = 0.001$, **$p = 0.002$ and *$p = 0.033$. **f**, **m** SUM159 and MDA-MB-231 cells were incubated with V9302 (0, 5, 10 and 20 μM) for 72 h. Total GSH was measured using an assay kit and end-point reading method. **g**, **n** After 72 h treatment with V9302, cells were collected and incubated with ROS detection reagent (1 μM) using an Enzo ROS-1D Detection Kit. ROS levels were measured using flow cytometry.

transporters induce ferroptosis in TNBC. Glutamine transporters such as ASCT2 is highly expressed in TNBC patients and play a vital role in TNBC cell growth [19]. In this study, we observed that the ASCT2 gene (*SLC1A5*) along with 50% of the SNAT family (*SLC38A*) of neutral amino acid transporters are highly expressed in TNBC patients. In addition, the significant association of *SLC1A5* with chemotherapy resistance and poor survival of breast cancer patients emphasises targeting glutamine metabolism for

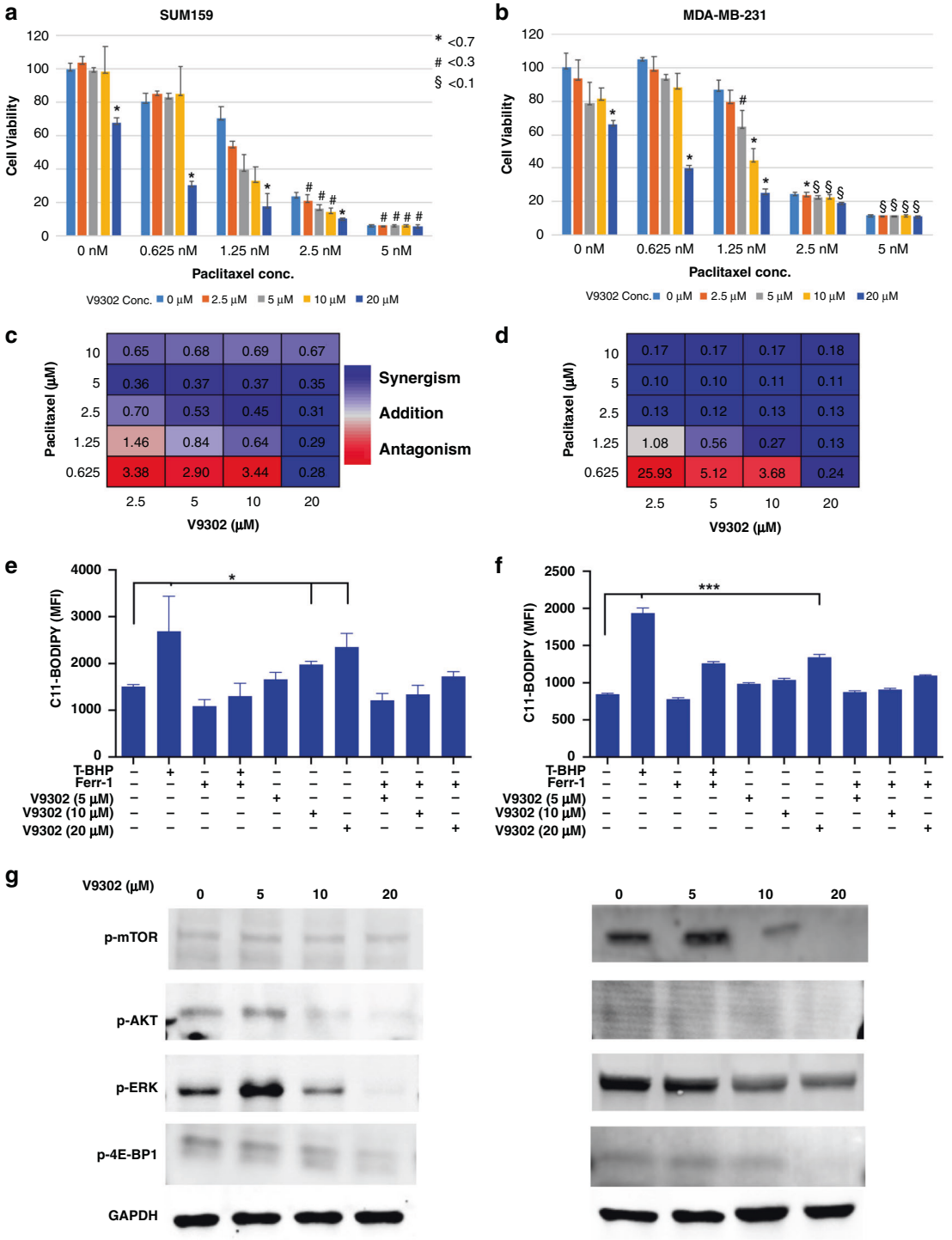

Fig. 5 V9302 induces synergistic killing and ferroptosis and inhibits the mTOR pathway in TNBC cells. a–d For synergy analysis, SUM159 and MDA-MB-231 cells were treated with paclitaxel (0, 0.625, 1.25, 5 and 10 nM) and V9302 (0, 2.5, 5 and 10 μM) individually or in combination at different concentrations for 72 h. The combination index (CI) was evaluated by combined dose–response curves fitted to Chou–Talalay lines. CI < 0.7 indicates weak synergistic interaction, whereas CI < 0.3 and <0.1 indicate moderate and strong synergistic interaction, respectively. **e**, **f** TNBC cells were treated with V9302 at different concentrations with or without ferrostatin-1 for 48 h. T-BHP, a ferroptosis inhibitor, was used as a positive control. Cells were stained with C11-BODIPY dye and analysed on a flow cytometry using the FL-1 channel. One-way ANOVA followed by Dunnett's post hoc test was performed for GD2 expression, taking untreated cells as the control. ***$p = 0.001$ and *$p = 0.033$. **g** Western blot analysis of SUM159 and MDA-MB-231 cells treated with V9302 (0, 5, 10 and 20 μM) for 24 h. The membranes were incubated with primary antibodies for p-AKT, p-ERK, p-mTOR and p-4E-BP1 at 1:500 dilution and GAPDH at 1:1000. Then, the membranes were incubated with respective fluorochrome-conjugated secondary antibodies at 1:3000 and scanned using a ChemiDoc Imaging System. The symbols, # and §, indicate Combination Index (CI) at different cutoff values (0.7, 0.3 and 0.1).

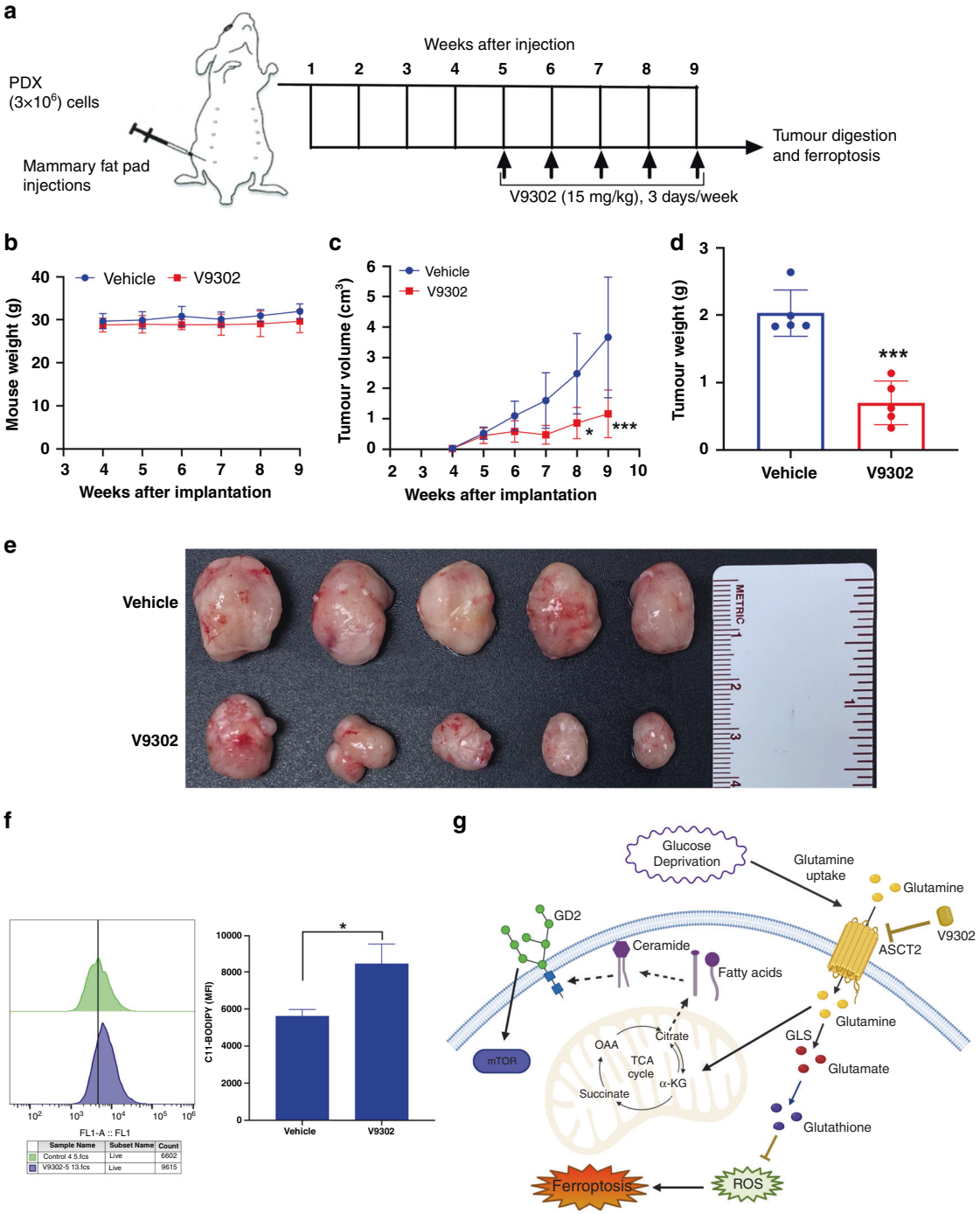

Fig. 6 Inhibition of glutamine metabolism reduces in vivo tumorigenesis. a Scheme of the treatment plan of mice injected with PDX cells. After the palpable tumours formed at week 5, mice were treated alone or in combination with V9302 (15 mg/kg) for 3 days per week. **b** Changes in the mouse weight from each group was monitored on weekly basis until the end of the study. **c**–**e** PDX cells were implanted (3×10^6 per mouse) into the mammary fat pads of NSG mice ($n = 20$, 5 mice per group). Once palpable tumours were formed, mice were randomly grouped into V9302 and vehicle control (2% DMSO in PBS) groups; V9302 treatment (15 mg/kg) was given thrice a week until the end of the study. After the tumour diameters reached 2 cm, mice were euthanized for tumour visualisation; shown are the tumours at 9 weeks after the implantation and tumour weights were measured. One-way ANOVA with Bonferroni's multiple comparison test was performed for tumour volumes, $*p < 0.05$ and $***p < 0.001$. An unpaired t test was performed for the tumour weights, $***p < 0.001$. **f** In vivo ferroptosis on the cells isolated from the PDX tumours obtained from mice treated with vehicle or V9302. Lipid peroxide levels were measured by C11-BODIPY staining using flow cytometry. An unpaired t test was performed between untreated and V9302-treated tumour cells. $*p = 0.033$. **g** Summarised illustration of metabolic stress-inducing glutamine uptake that may contribute to GD2 biosynthesis through TCA cycle and fatty acid synthesis (dotted arrows). Glutamine is required for glutathione synthesis and homeostasis of ROS. However, inhibition of ASCT2 by V9302 not only downregulate GD2 expression but also inhibits glutathione production and induces ferroptosis.

therapeutics development. Glutamine metabolism is also critical in activating the mTOR-mediated nutrient-sensing pathway to regulate cell growth and progression of cancer cells [19, 35]. Recently, we demonstrated that GD3 synthase regulates tumour growth and metastasis in TNBC via the FAK-AKT-mTOR pathway [24, 25]. Therefore, it is obvious from our study that targeting glutamine transporters by V9302 inhibited the glutamine uptake resulting in reduced GD2 expression and downregulation of the AKT-mTOR pathway (Fig. 6g).

Our study is confined to understanding the role of metabolic stress on the $GD2^+$ BCSC phenotype and nutrient substrates contributing to GD2 biosynthesis in the absence of glucose. Further studies will complement our understanding of the impact of GD2 on the recruitment of immune cells to the tumour microenvironment. Given that glutamine is the major source of other biomolecules, inhibition of glutamine uptake may result in adverse effects that need to be further investigated. Moreover, the transport of glutamine by multiple transporters and the availability of amino acids such as asparagine may compensate and satisfy essential metabolic requirements of BCSCs. A variant of ASCT2 specific to mitochondria was recently reported and its interaction with V9302 need to be explored [14]. To the best of our knowledge, this is the first study to report that glutamine plays a vital role in the biosynthesis of GD2 and maintenance of the $GD2^+$ BCSC phenotype in TNBC. Our study provides insights into the molecular targets for $GD2^+$ BCSCs that can help in the development of novel therapeutic strategies for the treatment of TNBC.

REFERENCES

1. Bauer KR, Brown M, Cress RD, Parise CA, Caggiano V. Descriptive analysis of estrogen receptor (ER)-negative, progesterone receptor (PR)-negative, and HER2-negative invasive breast cancer, the so-called triple-negative phenotype: a population-based study from the California cancer Registry. Cancer. 2007; 109:1721–8.
2. Sharma P. Biology and management of patients with triple-negative breast cancer. Oncologist. 2016;21:1050–62.
3. Cluntun AA, Lukey MJ, Cerione RA, Locasale JW. Glutamine metabolism in cancer: understanding the heterogeneity trends. Cancer. 2017;3:169–80.
4. Ahmadiankia N, Bagheri M, Fazli M. Nutrient deprivation modulates the metastatic potential of breast cancer cells. Rep Biochem Mol Biol. 2019;8:139–46.
5. Sancho P, Barneda D, Heeschen C. Hallmarks of cancer stem cell metabolism. Br J Cancer. 2016;114:1305–12.
6. Liu P, Liao J, Tang Z, Wu W, Yang J, Zeng Z, et al. Metabolic regulation of cancer cell side population by glucose through activation of the Akt pathway. Cell Death Differ. 2014;21:124–35.
7. Munir R, Lisec J, Swinnen JV, Zaidi N. Lipid metabolism in cancer cells under metabolic stress. Br J Cancer. 2019;120:1090–8.
8. Aykin-Burns N, Ahmad IM, Zhu Y, Oberley LW, Spitz DR. Increased levels of superoxide and H_2O_2 mediate the differential susceptibility of cancer cells versus normal cells to glucose deprivation. Biochem J. 2009;418:29–37.
9. Simons AL, Mattson DM, Dornfeld K, Spitz DR. Glucose deprivation-induced metabolic oxidative stress and cancer therapy. J Cancer Res Ther. 2009;5:S2–6. Suppl 1.
10. Altman BJ, Stine ZE, Dang CV. From Krebs to clinic: glutamine metabolism to cancer therapy. Nat Rev Cancer. 2016;16:619–34.
11. Sun X, Wang M, Wang M, Yu X, Guo J, Sun T, et al. Metabolic reprogramming in triple-negative breast cancer. Front Oncol. 2020;10:428.
12. Qie S, Yoshida A, Parnham S, Oleinik N, Beeson GC, Beeson CC, et al. Targeting glutamine-addiction and overcoming CDK4/6 inhibitor resistance in human esophageal squamous cell carcinoma. Nat Commun. 2019;10:1296.
13. Wang JB, Erickson JW, Fuji R, Ramachandran S, Gao P, Dinavahi R, et al. Targeting mitochondrial glutaminase activity inhibits oncogenic transformation. Cancer Cell. 2010;18:207–19.
14. Yoo HC, Park SJ, Nam M, Kang J, Kim K, Yeo JH, et al. A variant of SLC1A5 is a mitochondrial glutamine transporter for metabolic reprogramming in cancer cells. Cell Metab. 2020;31:267.
15. Qie S, Liang D, Yin C, Gu W, Meng M, Wang C, et al. Glutamine depletion and glucose depletion trigger growth inhibition via distinctive gene expression reprogramming. Cell Cycle. 2012;11:3679–90.
16. Welbourne TC. Ammonia production and glutamine incorporation into glutathione in the functioning rat kidney. Can J Biochem. 1979;57:233–7.
17. Lampa M, Arlt H, He T, Ospina B, Reeves J, Zhang B, et al. Glutaminase is essential for the growth of triple-negative breast cancer cells with a deregulated glutamine metabolism pathway and its suppression synergizes with mTOR inhibition. PLoS ONE. 2017;12:e0185092.
18. Gross MI, Demo SD, Dennison JB, Chen L, Chernov-Rogan T, Goyal B. et al. Antitumor activity of the glutaminase inhibitor CB-839 in triple-negative breast cancer. Mol Cancer Ther. 2014;13:890–901.
19. van Geldermalsen M, Wang Q, Nagarajah R, Marshall AD, Thoeng A, Gao D. et al. ASCT2/SLC1A5 controls glutamine uptake and tumour growth in triple-negative basal-like breast cancer. Oncogene. 2016;35:3201–8.
20. Park S-Y, Choi J-H, Nam J-S. Targeting cancer stem cells in triple-negative breast cancer. Cancers. 2019;11:965
21. De Francesco EM, Sotgia F, Lisanti MP. Cancer stem cells (CSCs): metabolic strategies for their identification and eradication. Biochem J. 2018;475:1611–34.
22. Battula VL, Shi Y, Evans KW, Wang R-Y, Spaeth EL, Jacamo RO, et al. Ganglioside GD2 identifies breast cancer stem cells and promotes tumorigenesis. J Clin Investig. 2012;122:2066–78.
23. Ly S, Anand V, El-Dana F, Nguyen K, Cai Y, Cai S, et al. Anti-GD2 antibody dinutuximab inhibits triple-negative breast tumor growth by targeting GD2+ breast cancer stem-like cells. J Immunother. Cancer. 2021;9:e001197.
24. Shao C, Anand V, Andreeff M, Battula VL. Ganglioside GD2: a novel therapeutic target in triple-negative breast cancer. Ann NY Acad Sci. 2021:1–19. Epub ahead of print.
25. Nguyen K, Yan Y, Yuan B, Dasgupta A, Sun J, Mu H, et al. ST8SIA1 regulates tumor growth and metastasis in TNBC by activating the FAK–AKT–mTOR signaling pathway. Mol Cancer Ther. 2018;17:2689–701.
26. Yadav UP, Singh T, Kumar P, Sharma P, Kaur H, Sharma S, et al. Metabolic adaptations in cancer stem cells. Front Oncol. 2020;10:1010.
27. Amara CS, Ambati CR, Vantaku V, Badrajee Piyarathna DW, Donepudi SR, Ravi SS, et al. Serum metabolic profiling identified a distinct metabolic signature in bladder cancer smokers: a key metabolic enzyme associated with patient survival. Cancer Epidemiol Biomark Prev. 2019;28:770–81.
28. Arnold JM, Gu F, Ambati CR, Rasaily U, Ramirez-Pena E, Joseph R. et al. UDP-glucose 6-dehydrogenase regulates hyaluronic acid production and promotes breast cancer progression. Oncogene. 2020;39:3089–101.
29. Martinez AM, Kim A, Yang WS. Detection of ferroptosis by BODIPY 581/591 C11. Methods Mol Biol. 2020;2108:125–30.
30. Rey O, Young SH, Jacamo R, Moyer MP, Rozengurt E. Extracellular calcium sensing receptor stimulation in human colonic epithelial cells induces intracellular calcium oscillations and proliferation inhibition. J Cell Physiol. 2010;225:73–83.
31. Echeverria GV, Ge Z, Seth S, Zhang X, Jeter-Jones S, Zhou X, et al. Resistance to neoadjuvant chemotherapy in triple-negative breast cancer mediated by a reversible drug-tolerant state. Sci Transl Med. 2019;11:eaav0936.
32. Schulte ML, Fu A, Zhao P, Li J, Geng L, Smith ST, et al. Pharmacological blockade of ASCT2-dependent glutamine transport leads to antitumor efficacy in preclinical models. Nat Med. 2018;24:194–202.
33. Broer A, Fairweather S, Broer S. Disruption of amino acid homeostasis by novel ASCT2 inhibitors involves multiple targets. Front Pharmacol. 2018;9:785.
34. Edwards DN, Ngwa VM, Raybuck AL, Wang S, Hwang Y, Kim LC, et al. Selective glutamine metabolism inhibition in tumor cells improves antitumor T lymphocyte activity in triple-negative breast cancer. J Clin Invest. 2021;131.
35. Ueng SH, Chen SC, Chang YS, Hsueh S, Lin YC, Chien HP, et al. Phosphorylated mTOR expression correlates with poor outcome in early-stage triple negative breast carcinomas. Int J Clin Exp Pathol. 2012;5:806–13.
36. Lee E, Yang J, Ku M, Kim NH, Park Y, Park CB, et al. Metabolic stress induces a Wnt-dependent cancer stem cell-like state transition. Cell Death Dis. 2015;6:e1805.
37. Schug ZT, Peck B, Jones DT, Zhang QF, Grosskurth S, Alam IS, et al. Acetyl-CoA Synthetase 2 promotes acetate utilization and maintains cancer cell growth under metabolic stress. Cancer Cell. 2015;27:57–71.
38. White E. Role of the metabolic stress responses of apoptosis and autophagy in tumor suppression. Ernst Scher Found Symp Proc. 2007;4:23–34.
39. Caino MC, Chae YC, Vaira V, Ferrero S, Nosotti M, Martin NM, et al. Metabolic stress regulates cytoskeletal dynamics and metastasis of cancer cells. J Clin Invest. 2013;123:2907–20.
40. van den Bijgaart RJE, Kroesen M, Wassink M, Brok IC, Kers-Rebel ED, Boon L, et al. Combined sialic acid and histone deacetylase (HDAC) inhibitor treatment upregulates the neuroblastoma antigen GD2. J Biol Chem. 2019;294:4437–49.
41. Moons SJ, Adema GJ, Derks MT, Boltje TJ, Bull C. Sialic acid glycoengineering using N-acetylmannosamine and sialic acid analogs. Glycobiology. 2019;29:433–45.
42. Schnaar RL, Gerardy-Schahn R, Hildebrandt H. Sialic acids in the brain: gangliosides and polysialic acid in nervous system development, stability, disease, and regeneration. Physiol Rev. 2014;94:461–518.
43. Teoh ST, Ogrodzinski MP, Ross C, Hunter KW, Lunt SY. Sialic acid metabolism: a key player in breast cancer metastasis revealed by metabolomics. Front Oncol. 2018;8:174.

44. Schomel N, Hancock SE, Gruber L, Olzomer EM, Byrne FL, Shah D, et al. UGCG influences glutamine metabolism of breast cancer cells. Sci Rep. 2019;9:15665.
45. Luo Z, Xu J, Sun J, Huang H, Zhang Z, Ma W, et al. Co-delivery of 2-deoxyglucose and a glutamine metabolism inhibitor V9302 via a prodrug micellar formulation for synergistic targeting of metabolism in cancer. Acta Biomater. 2020;105:239–52.
46. Esaki N, Ohkawa Y, Hashimoto N, Tsuda Y, Ohmi Y, Bhuiyan RH, et al. ASC amino acid transporter 2, defined by enzyme-mediated activation of radical sources, enhances malignancy of GD2-positive small-cell lung cancer. Cancer Sci. 2018; 109:141–53.
47. Desideri E, Vegliante R, Cardaci S, Nepravishta R, Paci M, Ciriolo MR. MAPK14/p38alpha-dependent modulation of glucose metabolism affects ROS levels and autophagy during starvation. Autophagy. 2014;10:1652–65.
48. Lettieri-Barbato D, Aquilano K. Pushing the limits of cancer therapy: the nutrient game. Front Oncol. 2018;8:148.
49. Verma N, Vinik Y, Saroha A, Nair NU, Ruppin E, Mills G, et al. Synthetic lethal combination targeting BET uncovered intrinsic susceptibility of TNBC to ferroptosis. Sci Adv. 2020;6(34):eaba8968.
50. Seibt TM, Proneth B, Conrad M. Role of GPX4 in ferroptosis and its pharmacological implication. Free Radic Biol Med. 2019;133:144–52.

ACKNOWLEDGEMENTS

We are grateful to the patients who provided tumour biopsies for PDX model establishment. PDX models and derivatives were obtained from the Cazalot Breast Cancer Model Resource at The University of Texas MD Anderson Cancer Center. This resource was established through a gift from the Cazalot family and from funds from the MD Anderson Cancer Center Breast Cancer Moon Shot Programme. Editorial support was provided by Sunita Patterson and Bryan Tutt in Editing Services, Research Medical Library, MD Anderson Cancer Center. This study was supported by the Department of Defense (DOD), Grant #BC181493 (to VLB) and a Breast Cancer Research Foundation (BCRF) grant (to MA). Metabolomics and data analysis were performed by Metabolomics core facility, Baylor College of Medicine. This project was supported by CPRIT Proteomics and Metabolomics Core Facility (to NP), (RP170005), National Institute of Health (NIH)/National Cancer Institute (NCI) grant (P30 CA125123), Dan L. Duncan Cancer Center and NIH/NCI R01CA220297 (to NP) and NIH/NCI R01CA216426 (to NP). Additional funding sources that supported this work include Cancer Prevention and Research Institute of Texas grants RP150148 (to HP-W).

AUTHOR CONTRIBUTIONS

AJ and VLB conceived the ideas, designed experiments, interpreted data and wrote the manuscript with inputs from all authors. AJ, SL and KN performed a majority of the experiments. BY assisted with Western blot and animal experiments. VA performed flow cytometry, qPCR and mammosphere assays. FE-D and ZA assisted with qPCR and mammosphere assays. DWBP and NP performed experiments and analyses pertaining to metabolomics. YY performed bioinformatics and combination index analysis. HP-W contributed to TNBC PDX models. HCM contributed V9302. MA and VLB supervised and directed all aspects of the study.

COMPETING INTERESTS

The authors declare no competing interests.

ETHICS APPROVAL AND CONSENT TO PARTICIPATE

This study was performed in accordance with the Declaration of Helsinki. All experiments involving animals were approved by and conducted in accordance with the policies of the Institutional Animal Care and Use Committee (IACUC) of The University of Texas MD Anderson Cancer Center.

ADDITIONAL INFORMATION

Supplementary information The online version contains supplementary material available at https://doi.org/10.1038/s41416-021-01636-y.

Correspondence and requests for materials should be addressed to V. Lokesh Battula.

Reprints and permission information is available at http://www.nature.com/reprints

Publisher's note Springer Nature remains neutral with regard to jurisdictional claims in published maps and institutional affiliations.